

# Elastic suppression of boiling in network fluids: a mechanism for hard-to-boil massecuite

Matthew G. Hennessy<sup>a,b,1,\*</sup>, Iain R. Moyles<sup>c,1</sup>, Stuart J. Thomson<sup>d,1</sup>

<sup>a</sup>*Mathematical Institute, University of Oxford, Andrew Wiles Building, Radcliffe Observatory Quarter, Woodstock Road, Oxford, OX2 6GG, United Kingdom*

<sup>b</sup>*Centre de Recerca Matemàtica, Campus de Bellaterra, Edifici C, 08193 Bellaterra (Barcelona), Spain*

<sup>c</sup>*Mathematics Applications Consortium for Science and Industry, Department of Mathematics and Statistics, University of Limerick, Limerick, Ireland*

<sup>d</sup>*Department of Mathematics, Massachusetts Institute of Technology, Cambridge, MA, 02139-4307, USA*

---

## Abstract

Massecuite is a liquid mixture that is boiled to produce raw sugar. When formed from poor-quality sugar cane, massecuite can be difficult to boil, leading to factory shutdowns lasting several weeks. This “hard-to-boil” (HTB) massecuite is rich in long-chained polysaccharides and thus exhibits a rheology that is dominated by elasticity. We examine how the rheology of massecuite affects the onset of boiling by proposing an extension of classical nucleation theory that accounts for the elastic energy of fluids containing a deformable solid network. The elasticity of a fluid is shown to suppress the onset of boiling through an increase in the boiling temperature, which is calculated to be a linear function of the shear modulus. Using experimental data, the model correctly predicts that regular and HTB massecuite should and should not boil under standard operating conditions. By coupling the boiling problem to a heat transfer model, the thermorheological properties of HTB massecuite are shown to greatly increase the time it takes to reach the boiling temperature. We propose further experiments that can be used to validate the theoretical results obtained here.

**Keywords:** Boiling, nucleation theory, elasticity, massecuite, heat transfer, mathematical modelling

---

## 1. Introduction

Massecuite is a dense mass of sugar crystals mixed with mother liquor obtained after sugar juice evaporation. It is a common and important source of raw sugar and molasses in sugarcane processing. Raw sugar is formed when the massecuite syrup is boiled to increase sucrose concentration. The dissolved sucrose molecules can then deposit onto sugar crystals, causing their growth. In South Africa and the United States

---

\*Corresponding author

Email addresses: [hennessy@maths.ox.ac.uk](mailto:hennessy@maths.ox.ac.uk) (Matthew G. Hennessy), [iain.moyles@ul.ie](mailto:iain.moyles@ul.ie) (Iain R. Moyles), [thomsons@mit.edu](mailto:thomsons@mit.edu) (Stuart J. Thomson)

<sup>1</sup>These authors contributed equally to this work.

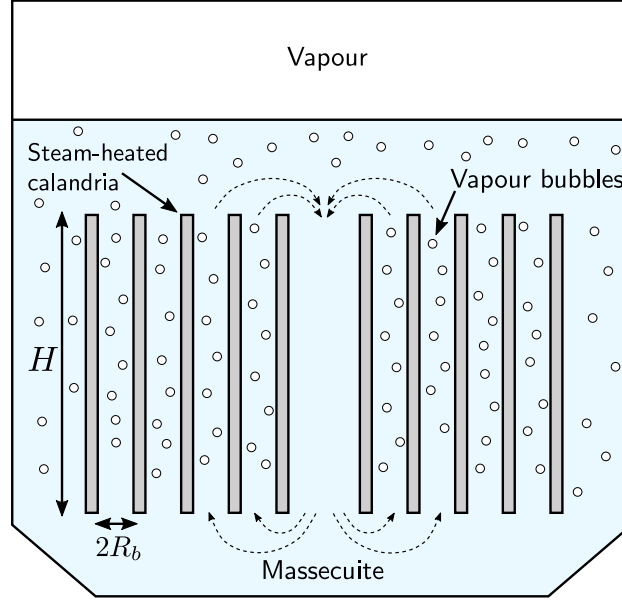


Figure 1: Cross section of a typical pan used to evaporate water from massecuite. A steam-heated calandria raises the temperature of the massecuite, causing it to boil. The nucleated vapour bubbles drive an upwards circulation flow due to buoyancy. The vapours bubbles escape through the massecuite surface and the fluid sinks downwards at the center of the pan.

alone, over \$3 billion USD of revenue is generated annually and over 15 million tonnes of sugar are produced each season [1, 2].

Massecuite processing happens in large evapo-crystallizers, or “pans”, that are typically cylindrical in nature. Within the pan is a steam-heated calandria (see Fig. 1) that is used to increase the temperature of the massecuite and initiate the boiling process. The calandria is a large metal heat exchanger consisting of roughly 1,200 open vertical tubes through which massecuite can flow. Each tube has a circular cross section of radius  $R_b = 5$  cm and a height of  $H = 1$  m. The massecuite inside these tubes boils and the nucleated bubbles drive an upwards flow due to buoyancy. The vapour bubbles then escape through the surface and the massecuite then sinks, resulting in a circulation flow [3]. To facilitate boiling, the entire pan is held below atmospheric pressure. While this boiling process is generally robust, slow boiling problems have been encountered due to “hard-to-boil” (HTB) massecuite, which generally occurs when poor-quality sugarcane is delivered to the processing factory. The suppression of boiling in massecuite is particularly problematic because the fluid is unable to flow through the boiler without the formation of vapour bubbles. The consequences of stagnant HTB massecuite can be severe, leading to factory shutdowns lasting several weeks [4].

Despite the aforementioned negative economic implications, the problem of HTB massecuite has received relatively little attention [4–7] and a consensus on how it negatively impacts the boiling process is yet to be resolved. To identify the key factors which prevent the boiling of massecuite, Eggleston *et al.* [4] have

carried out a comprehensive study to examine and contrast the physical characteristics of normal and HTB massecuite. They report that HTB massecuite (i) has significantly reduced thermal conductivities and heat transfer coefficients, and (ii) can exhibit viscoelastic rheology due to the presence of an intermolecular gel-like network that is formed by long-chained polysaccharides. The polysaccharide network can play a secondary role and entrap vapour bubbles that are too large, inhibiting the buoyancy-driven circulation flow, and making it appear as if the massecuite is not boiling [4].

Experimental measurements place the shear modulus of HTB massecuite in the range of 100 kPa, which, as will be shown below, is about 10 to 100 times greater than that of regular massecuite [4]. The strong elasticity of HTB massecuite can alter the energetic requirements for the nucleation of a vapour bubble to occur. According to classical nucleation theory [8, 9], which does not consider elastic effects, the radius of the nucleated bubble must be sufficiently large that the energy released from the phase transformation offsets the energy required to form a liquid-vapour interface. In the case of a bubble nucleating in a network fluid such as HTB massecuite, there is a second energy barrier that must be overcome; this is the elastic energy required to deform the solid network due to the volumetric expansion of liquid as it transforms into vapour. To offset the elastic energy, additional energy must be released by the phase transition. This can only be achieved by further superheating of the fluid. In the context of HTB massecuite, where the temperature of the fluid is limited by the transfer of heat from the calandria, obtaining the required level of superheating may not be possible. An insufficient level of superheating would either lead to a complete suppression of boiling or increase the size of nucleated bubbles, making them more likely to become trapped within the polysaccharide network. Difficulties in reaching the required level of superheating may also be compounded by reductions in the heat transfer coefficient and thermal conductivity of HTB massecuite.

The role of elasticity in the nucleation of gas bubbles appears to have been first studied by Gent and Tompkins [10]. By carrying out experiments with elastomers that were supersaturated with gas, they found that the critical saturation pressure that is necessary for bubble nucleation is linearly proportional to the elastic modulus. Stewart [11] and Kim *et al.* [12] developed theories of homogeneous nucleation of gas bubbles in supersaturated elastomers. However, in neither of these studies is the elastic energy considered when formulating the critical conditions that lead to nucleation. Using a simple model, Guéna *et al.* [13] showed that the boiling temperature of a yield stress fluid increases linearly with the yield stress. The increase in boiling temperature due to elasticity is briefly discussed in Hetsroni *et al.* [14] and Rapoport *et al.* [15]; however, little attempt is made to quantify this relationship using theoretical or experimental approaches. Rykaczewski and Phadnis [16] use theoretical arguments to show that soft surfaces can reduce the amount of superheating required to initiate heterogeneous nucleation. Finally, motivated by applications in medicine, several studies have shown that elasticity can inhibit shock-induced cavitation of bubbles in soft tissue which are commonly assumed to exhibit viscoelastic behaviour [17–19]. The results and discussions contained in the aforementioned studies provide strong evidence to suggest that the elastic nature of HTB massecuite will

indeed influence its boiling characteristics. However, the theoretical framework that is required to establish the precise relationship between elasticity and bubble nucleation in superheated viscoelastic fluids such as massecuite is not well developed.

The goal of this paper is therefore three-fold. First, we propose a simple extension of classical nucleation theory that accounts for the nonlinear elastic response of a superheated network fluid. Secondly, we use this theory to determine whether the elasticity of HTB massecuite affects the temperature that leads to the onset of boiling. Moreover, the impact that elasticity has on the critical radius of nucleation is ascertained, which addresses the issue of whether vapour bubbles can become trapped in the polysaccharide network. Thirdly, we investigate how changes to the heat transfer coefficient and thermal conductivity affect the time it takes for HTB massecuite to reach the boiling temperature that was calculated using nucleation theory. Based on our results, we can then make recommendations for how to avoid HTB massecuite.

The outline of the paper is as follows. In §2, a model of homogeneous bubble nucleation in a network fluid is derived which accounts for vapourisation, surface, and elastic energies. In §3, we then develop a mathematical model for heat transfer in the pan and calculate the time it takes to reach the boiling temperature. Both the boiling temperature and time-to-boil are expressed in terms of massecuite properties. The results of these models along with their implications for boiling and future experiments are discussed in §4. Conclusions and avenues for future work appear in §5.

## 2. Homogeneous nucleation of vapour bubbles in a network fluid

We consider the homogeneous nucleation of a spherical vapour bubble in an infinite bath of network fluid. The fluid is assumed to consist of a volatile incompressible liquid phase and a deformable incompressible elastic network. The elastic network is embedded within the volatile liquid and enables the displacement and hence strain of material elements to be defined [20]. In order for nucleation to occur, the fluid must be in a superheated state with temperature  $T > T_{\text{vap}}^0$ , where  $T_{\text{vap}}^0$  is the vapourisation (or boiling) temperature of the pure liquid (with zero elasticity). Although superheating is required for nucleation, we assume that we are sufficiently far from the superheat limit of the fluid which is approximately 90% the temperature at which a liquid phase can no longer exist (*i.e.*, the critical temperature) [21]. This is a reasonable assumption since we are in a hard-to-boil framework. Furthermore, sugar will undergo many phase transitions at high temperatures, a process which is essential for candy production, changing the rheology of the mixture [22]. Altering massecuite is not desired by refineries and many of the industrial processes are designed to prevent phase changes. For example, the pressures for many refining processes are chosen to reduce the boiling point of massecuite well-below 110–130 °C where caramelisation and colour formation occurs [23].

The volume of fluid undergoing vapourisation is assumed to be a sphere of radius  $R_v$ ; see Fig. 2. Since mass is conserved during phase change, the radius of the vapour bubble can be calculated as  $r_v =$

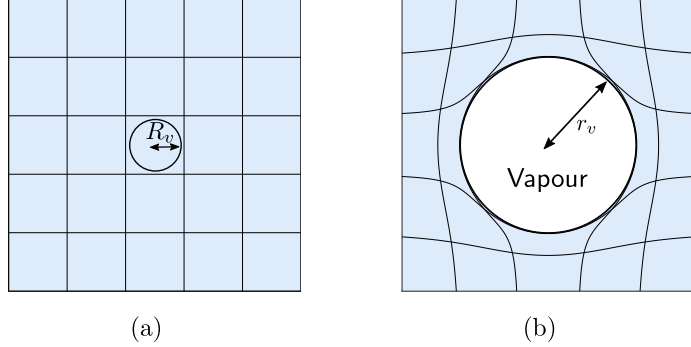


Figure 2: Bubble nucleation in a network fluid consisting of a volatile liquid and a deformable elastic network. When a spherical volume of liquid with radius  $R_v$  undergoes vaporisation [panel (a)], it expands to a sphere of radius  $r_v$  [panel (b)] due to the density of fluid being greater than the density of vapour. This expansion causes material elements to be displaced and deformed and requires additional energy.

$(\rho_l/\rho_v)^{1/3}R_v$ , where  $\rho_l$  and  $\rho_v$  denote the densities of the volatile liquid component and its vapour, respectively. It will be convenient to define the radial expansion of the vapourising liquid as

$$\lambda_0 = r_v/R_v = (\rho_l/\rho_v)^{1/3}. \quad (1)$$

To account for large deformations in the elastic matrix, the mechanics of the system are described using the framework of nonlinear elasticity (see Ref. [24, Chap. 5]). For simplicity, the elastic network is treated as an isotropic hyperelastic material with a strain energy density given by  $\mathcal{W}$ , which will be specified below. We assume that deformations are purely elastic and do not consider effects such as the finite extensibility of the network and irreversible plastic deformations.

We will begin in §2.1 with a discussion of the energetics of bubble nucleation in a network fluid. Then, as we shall see, this will allow us in §2.2 to derive a critical radius of nucleation which a newly formed bubble must exceed in order to continue growing as the fluid is heated.

### 2.1. Energetics of bubble nucleation

The change in free energy  $\Delta E$  that occurs upon nucleation of a spherical vapour bubble of radius  $r_v$  can be written as [25]

$$\Delta E = \rho_v V_v \Delta g_{\text{vap}} + \gamma_{lv} A_v + U_e, \quad (2)$$

where  $A_v = 4\pi r_v^2$  and  $V_v = (4/3)\pi r_v^3$  are the area and volume of the vapour nucleus, respectively,  $\Delta g_{\text{vap}}$  is the change in bulk chemical energy (per unit mass) due to vapourisation,  $\gamma_{lv}$  is the mean interfacial energy of a vapour-fluid interface, and  $U_e$  is the total elastic energy.

The change in the bulk chemical energy, *i.e.*, the bulk Gibbs free energy, can be written as  $\Delta g_{\text{vap}} = \Delta h(T) - T\Delta s(T)$ , where  $\Delta h$  and  $\Delta s$  are the temperature-dependent changes in enthalpy and entropy

per unit mass, respectively. Phase equilibrium at the vapourisation temperature  $T_{\text{vap}}^0$  requires  $\Delta g_{\text{vap}} = L_{\text{vap}} - T_{\text{vap}}^0 \Delta s(T_{\text{vap}}^0) = 0$ , where  $L_{\text{vap}} = \Delta h(T_{\text{vap}}^0)$  is the latent heat of vapourisation per unit mass. If we assume that the relative superheating  $T/T_{\text{vap}}^0 - 1$  is sufficiently small that the temperature dependence of the enthalpy and entropy can be neglected, then we obtain

$$\Delta g_{\text{vap}} = -L_{\text{vap}} \left( \frac{T}{T_{\text{vap}}^0} - 1 \right). \quad (3)$$

The form of (3) shows that energy is released upon vapourisation ( $\Delta g_{\text{vap}} < 0$ ) only when the fluid is superheated,  $T > T_{\text{vap}}^0$ .

In order to calculate the elastic energy  $U_e$ , we need to consider the deformation of the elastic matrix in response to the expansion of the vapour bubble. We begin by assuming that the displacement caused by nucleation is purely radial. Therefore, a material element initially at Lagrangian position  $\mathbf{X} = (R, \Theta, \Phi)$ , where  $R$ ,  $\Theta$ , and  $\Phi$  are spherical coordinates, is displaced to the Eulerian position  $\mathbf{x}(\mathbf{X}) = (r(R), \Theta, \Phi)$ . The function  $r(R)$  describing this displacement is to be determined. The corresponding deformation gradient tensor is given by  $\mathbf{F} = \partial \mathbf{x} / \partial \mathbf{X} = \text{diag}(dr/dR, r/R, r/R)$ . Incompressibility of the elastic network requires  $\det \mathbf{F} = 1$  and allows the strain energy density  $\mathcal{W}$  to be written as a function of the first and second invariants of the Green deformation tensor  $\mathcal{C} = \mathbf{F}^T \mathbf{F}$  given by

$$I_1 = \text{tr}(\mathcal{C}), \quad I_2 = \frac{1}{2} (\text{tr}(\mathcal{C})^2 - \text{tr}(\mathcal{C}^2)). \quad (4)$$

The elastic energy  $U_e$  of a hyperelastic material by definition is

$$U_e = 4\pi \int_{R_v}^{\infty} \mathcal{W}(I_1, I_2) R^2 dR. \quad (5)$$

Evaluating the elastic energy (5) requires the deformation gradient  $\mathbf{F}$  and hence the deformation  $r(R)$  to be fully determined. An explicit solution for  $r$  can be obtained from the incompressibility condition  $\det \mathbf{F} = 1$  and the boundary condition  $r(R_v) = r_v = \lambda_0 R_v$ , yielding  $r(R) = [R^3 + R_v^3 (\lambda_0^3 - 1)]^{1/3}$ .

To understand how  $U_e$  scales with the radius of the vapour bubble, the Lagrangian and Eulerian coordinates are non-dimensionalised by writing  $r = \lambda_0 R_v \tilde{r}$  and  $R = \lambda_0 R_v \tilde{R}$ . The elastic energy (5) can then be written as

$$U_e = 4\pi r_v^3 \mathcal{E}, \quad \mathcal{E} = \int_{\lambda_0^{-1}}^{\infty} \mathcal{W}(\tilde{I}_1, \tilde{I}_2) \tilde{R}^2 d\tilde{R}, \quad (6)$$

where  $\tilde{I}_i$  are the invariants (4) written in terms of  $\tilde{\mathbf{F}} = \text{diag}(d\tilde{r}/d\tilde{R}, \tilde{r}/\tilde{R}, \tilde{r}/\tilde{R})$  with  $\tilde{r} = (\tilde{R}^3 + 1 - \lambda_0^{-3})^{1/3}$ .

In summary, by inserting the components of the energy (3) and (6) into (2), the change in energy due to vapourisation is given by

$$\Delta E = -4\pi r_v^3 \left[ \frac{\rho_v L_{\text{vap}}}{3} \left( \frac{T}{T_{\text{vap}}^0} - 1 \right) - \mathcal{E} \right] + 4\pi r_v^2 \gamma_{lv}. \quad (7)$$

Using (7), we are now in a position to determine the critical radius which a newly formed bubble must reach in order to continue growing following nucleation.

### 2.2. Critical conditions for nucleation

A bubble that is nucleated in the fluid will continue to grow provided that energy is continually released during expansion of the bubble. This will happen provided a critical bubble radius,  $r_c$  is reached, corresponding to the radius at which further growth becomes energetically favourable (i.e.,  $\Delta E$  decreases). To find  $r_c$ , we maximise (7) with respect to  $r_v$ , which leads to

$$r_c = \frac{2\gamma_{lv}}{\rho_v L_{\text{vap}}(T/T_{\text{vap}}^0 - 1) - 3\mathcal{E}}. \quad (8)$$

From (8), increasing the strength of elastic effects (increasing  $\mathcal{E}$ ) leads to a corresponding increase in the critical radius required for nucleation. We note that Equation (8) can alternatively be expressed in terms of the critical radius of the liquid sphere that vapourises as

$$R_c = \frac{2\gamma_{lv}\lambda_0^2}{\rho_l L_{\text{vap}}(T/T_{\text{vap}}^0 - 1) - 3\lambda_0^3\mathcal{E}}, \quad (9)$$

which explicitly shows how the radial stretch  $\lambda_0 > 1$  induced by the density change also increases the effective surface energy that must be overcome during nucleation. By re-arranging (8) for  $T$ , we obtain a generalised Gibbs–Thomson condition for the interfacial temperature, which is similar to those derived from the thermodynamics of stressed solids [26, 27]. Bubble nucleation becomes impossible when  $r_c \rightarrow \infty$  (alternatively, when  $R_c \rightarrow \infty$ ), which defines a nucleation temperature  $T_{\text{nuc}}$  at which boiling can theoretically begin. This nucleation temperature is given by

$$T_{\text{nuc}} = T_{\text{vap}}^0 \left( 1 + \frac{3\mathcal{E}}{\rho_v L_{\text{vap}}} \right). \quad (10)$$

In the absence of elastic effects,  $\mathcal{E} = 0$ , the nucleation temperature coincides with the (inelastic) boiling temperature. However, as the elasticity of a material increases, greater temperatures are required to induce the formation of vapour bubbles and initiate boiling.

### 2.3. The case of Mooney-Rivlin fluids

To make further progress, we must select a particular form for the strain energy density  $\mathcal{W}$ . There are a number of possible constitutive laws that could be imposed, however, in the absence of more comprehensive rheological data for massecuite, we use the incompressible Mooney-Rivlin equation of state, which is a simple model that captures nonlinearities in the stress-strain curve due to large deformations. The Mooney-Rivlin strain energy density is given by

$$\mathcal{W}(\tilde{I}_1, \tilde{I}_2) = \frac{c_1}{2}(\tilde{I}_1 - 3) + \frac{c_2}{2}(\tilde{I}_2 - 3). \quad (11)$$

The elastic constants  $c_1$  and  $c_2$  are related to the shear modulus  $\mu$  via  $\mu = c_1 + c_2$ , and are assumed to be those of the fluid and not of the pure elastic material. We note by setting  $c_2 = 0$  in (11), we recover the neo-Hookean equation of state. In the context of nonlinear (finite-strain) viscoelasticity, the neo-Hookean

and Mooney-Rivlin constitutive relations are used to describe the elastic component of Maxwell fluids [24, Chap. 9.2.4]. To ensure that we investigate the influence of varying both  $c_1$  and  $c_2$  while maintaining the equality  $\mu = c_1 + c_2$  (required for consistency with the experimental data that is available for massecuite), we introduce a parameter  $\mathcal{M}$  that ranges from zero to one and define

$$c_1 = \mu(1 - \mathcal{M}), \quad c_2 = \mu\mathcal{M}. \quad (12)$$

Note that  $\mathcal{M} = 0$  corresponds to a neo-Hookean fluid, while  $0 < \mathcal{M} \leq 1$  represents a Mooney-Rivlin fluid.

The form of the Mooney-Rivlin strain energy density  $\mathcal{W}$  given by (11) means that computing the integral  $\mathcal{E}$  defined in (6) in closed form is somewhat cumbersome. However, to make further analytical progress, we can exploit the fact that the vapour density is small compared to the fluid density, and as a result the radial stretch  $\lambda_0$  is large. We then find that the integral  $\mathcal{E}$  can be approximated by (see Appendix A for details)

$$\mathcal{E} \simeq \frac{\mu}{2} \left[ (1 - \mathcal{M}) \left( \frac{5}{3} - \frac{2}{\lambda_0} \right) + \mathcal{M} \left( \lambda_0 - \frac{2}{3} \right) \right], \quad (13)$$

for  $\lambda_0 \gg 1$ . Inserting (13) into (8) gives the critical radius of nucleation  $r_c$  for a given temperature  $T > T_{\text{vap}}^0$ . Additionally, combining (13) and (10) shows that the nucleation temperature is given by

$$T_{\text{nuc}} \simeq T_{\text{vap}}^0 \left\{ 1 + \frac{\mu}{\rho_v L_{\text{vap}}} \left[ (1 - \mathcal{M}) \left( \frac{5}{2} - \frac{3}{\lambda_0} \right) + \mathcal{M} \left( \frac{3}{2} \lambda_0 - 1 \right) \right] \right\}. \quad (14)$$

Gent and Tompkins [10] studied the nucleation of gas bubbles in supersaturated elastomers. By assuming the elastomer has a neo-Hookean response, they derived an expression for the pressure inside a bubble as a function of its radius and the shear modulus of the elastomer. To compare our modelling results, namely (8) and (13), to those of Gent and Tompkins, we first convert temperature changes into pressure changes using the Clausius–Clapeyron relation. Then, by restricting our attention to neo-Hookean materials by setting  $\mathcal{M} = 0$  in (13) and then taking the limit as  $\lambda_0 \rightarrow \infty$ , we are able to recover, at leading order, the expression for the critical saturation pressure proposed by Gent and Tompkins (*i.e.*, Eqn. (1) in their paper in the limit as  $r_0/r \rightarrow 0$ ). Therefore, the model derived by Gent and Tompkins can be considered a particular case of the general theory presented here.

### 3. Influence of elasticity and thermal properties on the boiling time

The increase in nucleation temperature  $T_{\text{nuc}}$  due to elasticity leads to the possibility of increases in the time  $t_{\text{nuc}}$  that is required for a fluid to reach this temperature and thus begin to boil. In the case of HTB massecuite, the increase in  $t_{\text{nuc}}$  can be compounded by changes in its thermal properties as well. The purpose of this section is to develop a model that can be used to determine how the elasticity of HTB massecuite and variations in its thermal properties affect the boiling time  $t_{\text{nuc}}$  by considering a specific heating scenario. In particular, we consider the transient heating of massecuite contained within a single cylindrical column of



the calandria (see Fig. 1). The initial temperature of the fluid is denoted by  $T_a$  and is below its nucleation temperature  $T_{\text{nuc}}$ . The metal boundary of the column is in contact with steam and assumed to have a constant temperature  $T_s$ . In this section, it will be assumed that the nucleation temperature is below the steam temperature,  $T_{\text{nuc}} < T_s$ , so that boiling can be achieved.

In a typical calandria, the columns have radius  $R_b \simeq 0.050$  m and height  $H \simeq 1.0$  m. Due to the small aspect ratio of the column,  $R_b/H \ll 1$ , the transfer of thermal energy from the heated surface to the massecuite will predominantly be in the radial direction. As the massecuite is not yet boiling, there are no vapour bubbles to drive an upwards flow of fluid through the column by buoyancy. Therefore, we will not consider convection or other fluid motion in our model. The transfer of heat from the calandria wall at  $r = R_b$  to the massecuite will be modelled by Newton's law of cooling with an advective heat transfer coefficient  $h_a$ . The heating of the massecuite is assumed to be axisymmetric. Under these assumptions, the dimensionless temperature of massecuite,  $\hat{u} = (T - T_a)/(T_s - T_a)$ , will evolve according to

$$\frac{\partial \hat{u}}{\partial \hat{t}} = \frac{1}{\hat{r}} \frac{\partial}{\partial \hat{r}} \left( \hat{r} \frac{\partial \hat{u}}{\partial \hat{r}} \right), \quad (15a)$$

where  $\hat{t} = (\rho_f c_p R_b^2/k)^{-1} t$  and  $\hat{r} = r/R_b$  are the dimensionless time and radial coordinate with  $c_p$  and  $k$  being the specific heat capacity and thermal conductivity of the fluid, respectively. The non-dimensional boundary and initial conditions are

$$\frac{\partial \hat{u}}{\partial \hat{r}} = 0, \quad \hat{r} = 0, \quad (15b)$$

$$\frac{\partial \hat{u}}{\partial \hat{r}} = \alpha(1 - \hat{u}), \quad \hat{r} = 1, \quad (15c)$$

$$\hat{u} = 0, \quad \hat{t} = 0, \quad (15d)$$

where  $\alpha = h_a R_b/k$  is the Biot number. Using the parameters in Table 1, we find that  $\alpha$  lies in the range of 13 to 115. The largeness of  $\alpha$  implies (from (15c)) that the temperature gradient near the heated surface is very large. This corresponds to the situation of localised heating. The massecuite near the surface experiences a rapid (relative to the rate of thermal diffusion) increase in temperature while the temperature of the bulk fluid remains unchanged (since thermal diffusion has not yet transported heat to the interior).

In light of the previous discussion, we expect the fluid adjacent to the calandria wall to first reach the nucleation temperature. Therefore, the dimensionless boiling time  $\hat{t}_{\text{nuc}}$  can be implicitly defined in terms of the temperature profile  $\hat{u}(\hat{r}, \hat{t}; \alpha)$  by the equation

$$\hat{u}(1, \hat{t}_{\text{nuc}}; \alpha) = \hat{u}_{\text{nuc}}, \quad (16)$$

where  $\hat{u}_{\text{nuc}} = (T_{\text{nuc}} - T_a)/(T_s - T_a)$  is the dimensionless nucleation temperature. Therefore, the boiling time  $\hat{t}_{\text{nuc}}$  will be a function of two variables; the Biot number  $\alpha$ , which contains information about the thermal properties of the fluid, and the dimensionless nucleation temperature  $\hat{u}_{\text{nuc}}$ , which contains information about

Table 1: Parameter values associated with the boiling of HTB massecuite

Parameter	Description	Value	Source
$R_b$	Calandria column radius	0.050 m	Provided
$H$	Calandria column height	1.0 m	Provided
$\rho_f$	Massecuite density	1400 kg m <sup>-3</sup>	Ref. [23]
$\rho_l$	Water density (at 100 °C)	958 kg m <sup>-3</sup>	Ref. [28]
$\rho_v$	Vapour density (at 100 °C)	0.60 kg m <sup>-3</sup>	Refs. [29, 30]
$c_p$	Specific heat capacity	2000 J kg <sup>-1</sup> °C <sup>-1</sup>	Ref. [31]
$k$	Thermal conductivity	0.26–0.38 W m <sup>-1</sup> °C <sup>-1</sup>	Ref. [4]
$h_a$	Advective heat transfer coefficient	100–600 W m <sup>-2</sup> °C <sup>-1</sup>	Ref. [23]
$T_s$	Steam temperature	110 °C	Ref. [23]
$T_a$	Ambient massecuite temperature	55 °C	Ref. [23]
$T_{\text{vap}}^0$	Vapourisation temperature of pure liquid	70 °C	Ref. [23]
$L_{\text{vap}}$	Latent heat of vapourisation (at 100°C)	$2.3 \times 10^6$ J kg <sup>-1</sup>	Refs. [29, 32]
$\gamma_{lv}$	Water-vapour interfacial tension (at 70 °C)	0.065 N/m <sup>2</sup>	Ref. [33]
$\mu$	Shear modulus of HTB massecuite	$\sim 10^5$ Pa	Ref. [4]

the elasticity of the fluid. By exploiting the largeness of the Biot number, the (dimensional) boiling time can be approximated by

$$t_{\text{nuc}} \simeq \tau(T_{\text{nuc}}) \frac{\rho_f c_p k}{h_a^2}, \quad (17)$$

where  $\tau$  is a dimensionless function of  $T_{\text{nuc}}$  that must be computed numerically; see Appendix B for details. We emphasise that (17) is an approximation of the boiling time that is only valid in the context of stagnant HTB massecuite. Under normal operation involving regular massecuite, convective boiling dominates and the heat transfer model (15) would need to be adapted to include a flow term.

## 4. Results and discussion

### 4.1. The nucleation temperature of HTB massecuite

We first study how elasticity influences the nucleation temperature of massecuite using the expression in (14). The dominant volatile component of massecuite is most likely water. Using the parameters in Table 1, we find that the radial expansion due to density change is  $\lambda_0 \simeq 11.7$ . The pan that is used to heat massecuite is held below atmospheric pressure in order to reduce the temperature at which boiling occurs. The reported boiling temperature of regular massecuite is  $T_{\text{vap}}^0 = 70$  °C [23]. The temperature of the steam that heats the calandria is typically held at 110 °C [23]. Finally, to evaluate the nucleation temperature

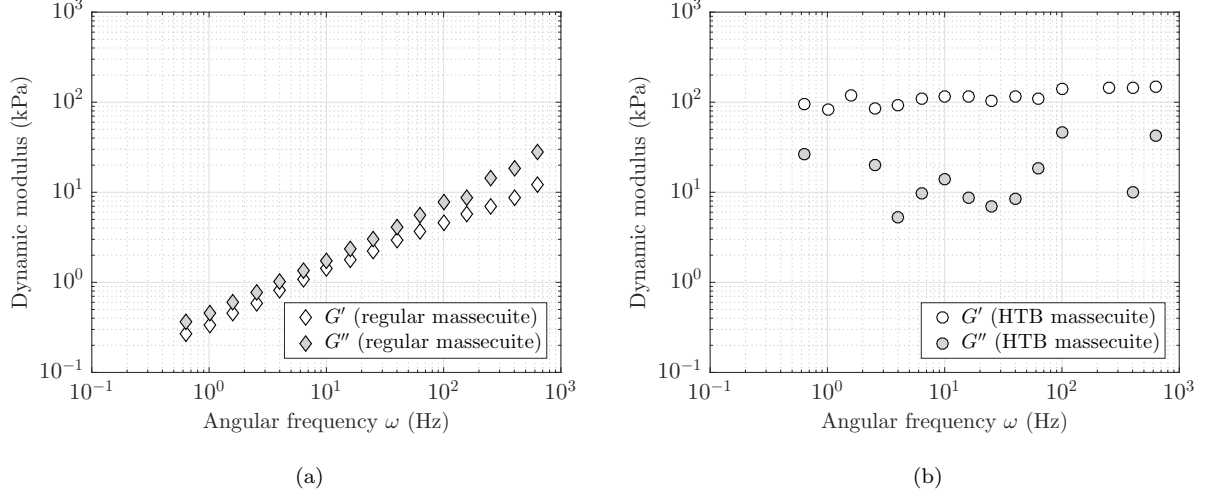


Figure 3: Measurements of the storage ( $G'$ ) and loss ( $G''$ ) moduli of regular (a) and HTB (b) massecuite obtained from an oscillatory deformation rheometer by Eggleston *et al.* [4]. The samples were held at 20 °C.

using (14), an estimation of the shear modulus  $\mu$  of massecuite is required. We now discuss how such an estimate can be obtained from rheological measurements.

The mechanical behaviour of regular and HTB massecuite has been measured using an oscillatory deformation rheometer by Eggleston *et al.* [4]. In these experiments, samples of massecuite held at 20 °C were subjected to sinusoidal deformations of angular frequency  $\omega$  and the resistance to motion was measured. From this data, the storage and loss moduli,  $G'$  and  $G''$ , respectively, could be measured. The storage and loss moduli characterise the elastic and viscous response of a viscoelastic material. Concentrated polymer solutions and gels are dominated by elastic effects and have  $G' > G''$  across all frequencies. Conversely, in dilute polymer solutions, the loss modulus dominates the storage modulus across all frequencies,  $G'' > G'$ . The frequency dependence of the dynamic moduli is shown in Fig. 3 for regular and HTB massecuite. The data shows that regular massecuite behaves as a dilute polymer solution and exhibits weak elastic effects, whereas HTB massecuite has gel-like rheology that is dominated by elasticity. Using the data in Fig. 3, we can obtain a rough approximation of the shear modulus  $\mu$  by setting it equal to the storage modulus  $G'$ ; thus,  $\mu \simeq G'$ . This approximation is exact when the loss modulus is equal to zero. Given that the storage modulus of HTB massecuite is roughly an order of magnitude larger than the loss modulus, we believe this is an accurate approximation in this case.

The calculated nucleation temperature (14) of regular and HTB massecuite is plotted as a function of shear modulus in Fig. 4. The elastic response of the massecuite has been assumed to be neo-Hookean with  $\mathcal{M} = 0$ . The role of elastic response will be discussed below. Our calculations show that the nucleation temperature of regular massecuite, which has a shear modulus that is less than 12 kPa, does not undergo significant increases from the reported boiling temperature of 70 °C. Furthermore, the nucleation temperature

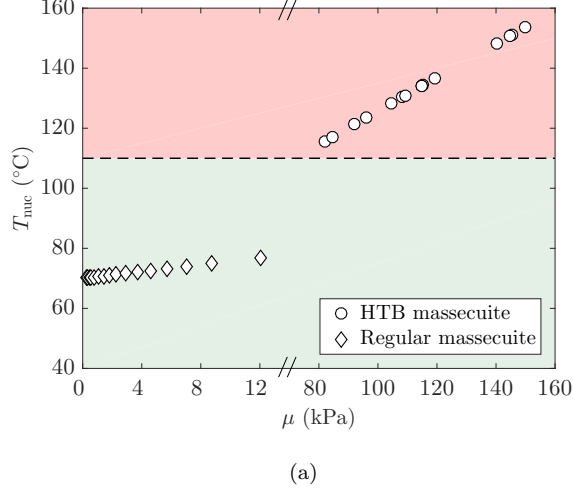


Figure 4: Estimation of the nucleation temperature for regular (circles) and HTB (diamonds) massecuite based on the experimental measurements of the storage modulus  $G'$  shown in Fig. 3. The massecuite has been assumed to have a neo-Hookean elastic response ( $\mathcal{M} = 0$ ). Green and red denote temperatures that are below and above the maximum temperature of typical boiling pans. The nucleation temperature has been calculated using (14) with parameter values in Table 1.

is much less than the temperature of the steam that is pumped through the calandria (110 °C), verifying that regular massecuite should boil under standard operating conditions. In the case of HTB massecuite, the nucleation temperature exhibits a strong linear dependence on the shear modulus. For all values of the shear modulus, our model predicts that the nucleation temperature of HTB massecuite is well above the steam temperature and thus should not be able to boil.

The estimation of the nucleation temperature strongly depends on the elastic response of the material and the degree of volumetric expansion that occurs upon vapourisation, which are characterised through the Mooney–Rivlin parameter  $\mathcal{M}$  and the radial stretch  $\lambda_0$ . The elastic stress of the polymer network may lead to a compression of the vapour bubble that results in a reduced value of  $\lambda_0$  and a greater vapour density  $\rho_v$  than reported in Table 1. To examine the role of the elastic response and the effects of vapour compressibility, the nucleation temperature of HTB massecuite has been re-calculated assuming a shear modulus of 100 kPa using a range of values for  $\mathcal{M}$  and  $\lambda_0$ . To account for values of  $\lambda_0$  that are close to one, the elastic energy  $\mathcal{E}$  defined in (6) is computed using numerical integration. The results are shown in Fig. 5 (a). For a fixed value of the  $\mathcal{M}$ , the nucleation temperature rapidly decreases with  $\lambda_0$  to the standard boiling temperature of 70 °C due to substantial weakening of elastic effects. The elastic response of the massecuite is only relevant for large values of the radial stretch,  $\lambda_0 > 5$ , where nonlinear mechanics become important. For smaller values of the radial stretch,  $\lambda_0 < 5$ , the value of the Mooney–Rivlin parameter  $\mathcal{M}$  has a negligible impact on the nucleation temperature. Given the strong dependence of the results on the value of the radial stretch, a thorough examination of the role of vapour compressibility during nucleation

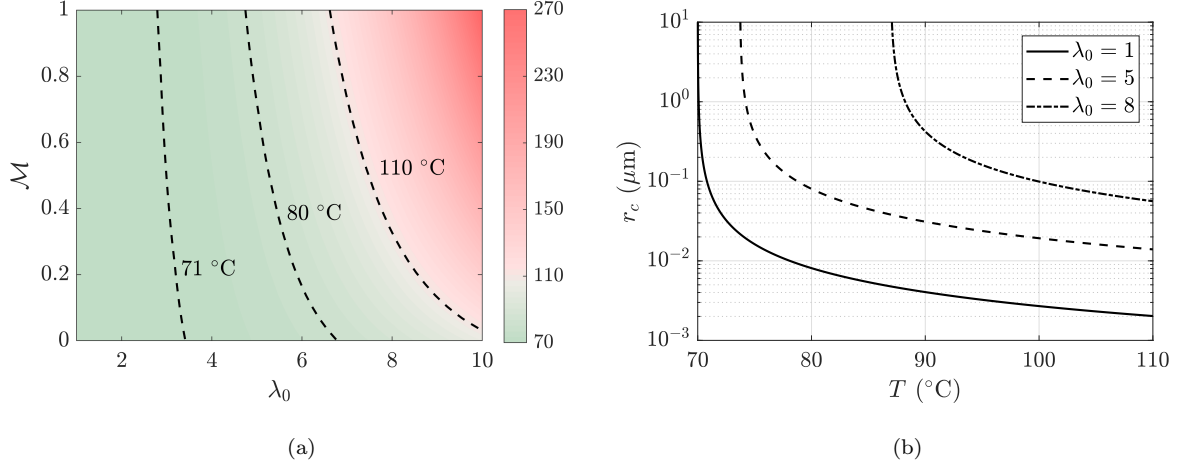


Figure 5: (a) The nucleation temperature as a function of the radial expansion  $\lambda_0$  and the Mooney–Rivlin parameter  $\mathcal{M}$ . Isotherms are shown for  $T_{\text{nuc}} = 71$  °C, 80 °C, and 110 °C. (b) The critical radius of nucleation as a function of temperature when  $\mathcal{M} = 0$  (neo-Hookean elastic response). Calculations are based on a shear modulus of 100 kPa.

may prove to be insightful. The works of Gaudron *et al.* [34] and Larché and Cahn [35, 36] may form the basis for an extended nucleation model that considers the detailed mechanics and thermodynamics of the vapour-fluid system.

Figure 5 (b) shows how the critical bubble radius given by (8) varies with temperature for various values of the radial stretch  $\lambda_0$ . The shear modulus is fixed at  $\mu = 100$  kPa, corresponding to HTB masseccuite. For each value of  $\lambda_0$ , the nucleation temperature is below the steam temperature and thus boiling can, in principle, take place. When  $\lambda_0 = 1$ , there is no volumetric expansion and hence the nucleation temperature coincides with the boiling temperature. In this case, the critical radius decreases from roughly one micron to a few nanometers as the steam temperature is approached. When the radial expansion is increased to  $\lambda_0 = 5$ , the nucleation temperature slightly increases to 74 °C. However, there are substantial increases in the critical radii of nucleation. Alternatively, a much greater amount of superheating is required to nucleate a bubble with the same radius compared to the case when  $\lambda_0 = 1$ . For instance, nucleating a bubble with a radius of 10 nm requires a superheat of 8 °C in the absence of elastic effects ( $\lambda_0 = 1$ ), but is impossible within the operating temperature range when  $\lambda_0 = 5$ . The increase in critical radius is even more severe when the radial stretch is increased to  $\lambda_0 = 8$ . In this case, it is only possible to nucleate bubbles that have a radius greater than 50 nm. To prevent nucleated bubbles from becoming trapped in the polysaccharide network that permeates HTB masseccuite, further increases in the temperature may be required. This would place the *apparent* boiling temperature of masseccuite beyond what can be obtained using standard industrial-scale boilers. The results of Fig. 5 indicate that elasticity can still play an important role in bubble nucleation even if the nucleation temperature does not undergo a substantial increase.

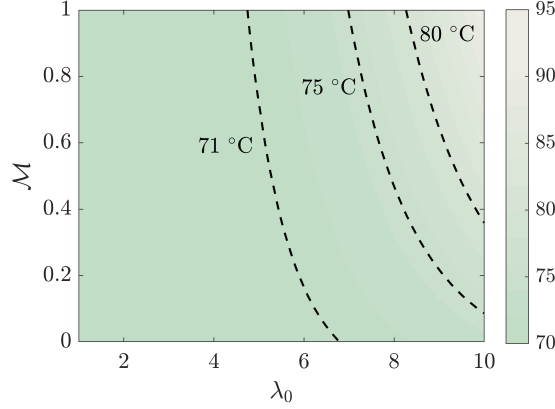


Figure 6: The nucleation temperature as a function of the radial expansion  $\lambda_0$  and the Mooney–Rivlin parameter  $\mathcal{M}$ . Isotherms are shown for  $T_{\text{nuc}} = 71$  °C, 75 °C, and 80 °C. Calculations are based on a reduced value of the shear modulus,  $\mu = 10$  kPa.

The estimations of the nucleation temperatures can be refined by accounting for the temperature dependence of the shear modulus. In the case of regular massecuite, the rheological properties at higher temperatures can be inferred from the measurements of Wang *et al.* [37]. These authors report that as the temperature increases from 20 °C to 80 °C, the storage modulus decreases by roughly one or two orders of magnitude, depending on the rheometer frequency used in obtaining the measurements. This decrease does not lead to substantial changes in the predicted nucleation temperature of regular massecuite because this was already calculated to be close to the (inelastic) vapourisation temperature. It is more difficult to estimate how temperature affects the rheology of HTB massecuite. This is due to a lack of experimental data and uncertainty in the composition of the polysaccharide network. However, the dynamic moduli of HTB massecuite can be expected to undergo similar decreases as the temperature of the fluid increases. To explore the impact of a reduced shear modulus on the modelling results for HTB massecuite, we have computed the nucleation temperature for various values of the Mooney–Rivlin parameter  $\mathcal{M}$  and the radial stretch  $\lambda_0$  taking  $\mu = 10$  kPa, which is a factor of 10 smaller than the value measured at 20 °C. The results are shown in Fig. 6. Compared to the case of  $\mu = 100$  kPa (see Fig. 5 (a)), the impact of elasticity on the nucleation temperature is much less pronounced. However, the maximum predicted nucleation temperature, based on a Mooney–Rivlin response with  $\mathcal{M} = 1$  and a radial expansion of  $\lambda_0 = 10$ , is still 95 °C, which might be difficult to reach using conventional processing techniques. The significant variations in the nucleation temperature with the Mooney–Rivlin parameter further underscore the importance of having accurate information about the mechanical response of HTB massecuite.

The nucleation model proposed in §2 is based on the assumption that massecuite is an ideal mixture. That is, we have not considered in the energy balance (2) the energy of interaction between water molecules and long-chained polysaccharides. Favourable interactions between water molecules and polysaccharide

chains may result in an additional energy barrier that must be overcome for boiling to occur. To estimate the error in the predicted nucleation temperature of regular massecuite, which behaves as a dilute polymer solution, we follow the approach of Han and Dae Han [38], who developed an extension of classical nucleation theory that accounts for the energetic interactions between solvent molecules and polymer chains. Using the Flory–Huggins theory of solvent-polymer mixtures [39, Chap. 2], the change in free energy per unit mass due to molecular interactions can be approximated in the limit of dilute polymer as  $(RT/M_w)(1/2 - \chi)\phi_p^2$ , where  $R$  is the universal gas constant,  $M_w$  is the molecular weight of solvent (in this case assumed to be water),  $T$  is temperature,  $\chi$  is the interaction parameter, and  $\phi_p$  is the volume fraction of polymer. Bae *et al.* [40] provide data for the interaction parameter for water-polymer systems, finding that  $\chi$  ranges between 0.4 and 1.2. Using the mean value of  $\chi = 0.8$  and assuming that regular massecuite is about 10% polysaccharide chains, then we find that the free energy change (per unit mass) due to solvent-polymer interactions is about 8% of the energy that is released upon vapourisation when regular massecuite is superheated by only 1 K. The interaction energy will become increasingly negligible compared to the vapourisation energy as the superheating is increased. Thus, we can conclude that our estimates of the nucleation temperature for regular massecuite should be accurate to within a few percent.

In the context of boiling massecuite, it is more likely that vapour nuclei will form at the heated calandria walls by heterogeneous nucleation than in the bulk by homogeneous nucleation. The reason being that, at a surface, vapour nuclei will take the shape of spherical caps and will have smaller surface areas compared to full spheres. Less energy is required to form the interface of a spherical cap and the energy barrier that must be exceeded for spontaneous growth of vapour nuclei is reduced. In principle, the modelling framework developed in §2 can be extended to the case of heterogeneous nucleation. However, the calculation of the elastic energy becomes substantially more involved due to the presence of a solid boundary, corresponding to the calandria wall, which breaks the spherical symmetry of the problem.

To make progress towards understanding role of elasticity during heterogeneous nucleation, we consider the formation of a vapour bubble at the calandria wall whereby the contact angle  $\varphi$  formed at the solid-liquid-vapour remains constant during the expansion process. Since the angle  $\varphi$  is constant, the initial radius of the fluid  $R_v$  and the radius of the vapour bubble  $r_v$  are again linked by mass conservation through the expression  $R_v = \lambda_0^{-1}r_v$ . By dimensionality arguments, the elastic energy must have the form  $U_e = \mu r_v^3 f(\lambda_0, \varphi)$ , where  $f$  is a dimensionless function. Importantly, this shows that the elastic energy scales like the cube of the contact line radius  $r_v$ . Since the vapourisation energy  $U_{\text{vap}}$  will scale in the same way, we can expect that elasticity will influence the dynamics of heterogeneous nucleation in the same way as predicted in §2 for homogeneous nucleation. In particular, elasticity will suppress the onset of boiling until a nucleation temperature  $T_{\text{nuc}}$  that exceeds the vapourisation temperature  $T_{\text{vap}}^0$  is reached.

While the focus of the foregoing discussion has been on the nucleation phase of micron-size bubbles, we stress that the rheological properties of HTB massecuite may play an important role in the subsequent

growth of fledgling bubbles which have nevertheless attained the critical threshold radius  $r_c$ . In particular, using a modified Rayleigh–Plesset formulation for bubble growth in the presence of elasticity, Gaudron *et al.* [34] suggest that elastic forces continue to retard bubble growth beyond the nucleation phase. How strongly the elasticity influences growth depends on the precise details of the constitutive model employed. Furthermore, as the bubble continues to grow it is likely that viscosity acts in conjunction with elasticity to suppress further expansion. Modelling such as that proposed by Gaudron *et al.* could provide a framework in which to independently investigate the role of fluid viscosity and its influence relative to elasticity at various stages of the bubble’s lifetime.

#### 4.2. The boiling time of HTB massecuite

Having established how elasticity affects the temperature at which vapour bubbles can theoretically form, we now examine how changes in the thermal properties of massecuite influence the time it takes to reach the nucleation temperature. It is worth emphasising here that the proceeding discussion does not depend on the exact nature of the nucleation process. Equation (17) shows that the boiling time  $t_{\text{nuc}}$  can be factored into a contribution associated with the nucleation temperature given by  $\tau(T_{\text{nuc}})$  and a contribution that contains the thermal parameters of massecuite, which is given by  $\rho_f c_p k / h_a^2$ . Figure 7 (a) shows that the pre-factor  $\tau(T_{\text{nuc}})$  increases exponentially with the nucleation temperature. This leads to the boiling time increasing by two orders of magnitude as the nucleation temperature increases from 70 °C to 100 °C. As the nucleation temperature approaches the steam temperature, the boiling time takes infinitely long to reach. Figure 7 (b) shows how the post-factor  $\rho_f c_p k / h_a^2$ , which is equivalent to  $t_{\text{nuc}} / \tau(T_{\text{nuc}})$ , varies due to changes in the thermal conductivity  $k$  and the heat transfer coefficient  $h_a$ . As the thermal conductivity is increased for a fixed value of the heat transfer coefficient, there is a slight increase in the nucleation temperature. This is due to the fact that, as the thermal conductivity is increased, more thermal energy is transported into the bulk of the massecuite rather than accumulating and heating the massecuite that is adjacent to the surfaces of the calandria. Increases in the heat transfer coefficient for fixed values of the thermal conductivity lead to marked decreases in the boiling time. Overall, the variation in thermal properties can lead to the boiling time varying by nearly two orders of magnitude as well. When combined with elastic effects and changes in the nucleation temperature, our results indicate that the boiling time change by up to four orders of magnitude over this range of  $T_{\text{nuc}}$ .

#### 4.3. Experimental implications

Despite the fact that several authors have commented on the increase in boiling temperature that can result from elasticity [13–16], to our knowledge there appears to be no experimental data in the literature that can be used to further validate the theoretical results obtained here. Thus, in this section we will propose an experiment that might be able to probe the validity of the theory developed in this article. This



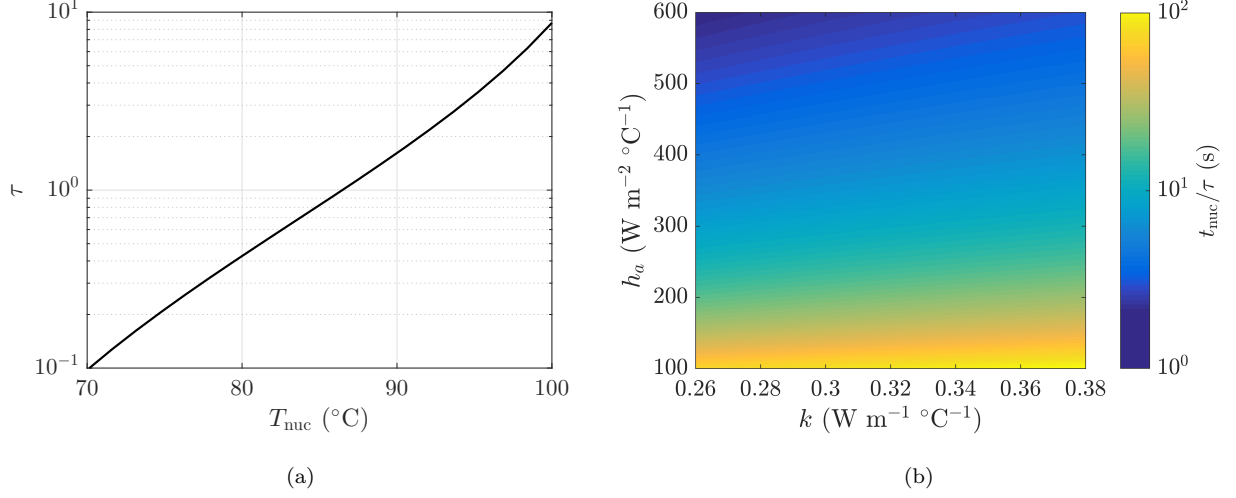


Figure 7: Predictions of how the boiling time  $t_{\text{nuc}}$  is influenced by elasticity and variations in the thermal properties of massecuite. (a) Variation of the pre-factor  $\tau$  in (17) with the nucleation temperature  $T_{\text{nuc}}$  and hence the elasticity of the massecuite. (b) Variations in the rescaled boiling time  $t_{\text{nuc}}/\tau$  with the thermal conductivity  $k$  and heat transfer coefficient  $h_a$ . For given values of  $T_{\text{nuc}}$ ,  $k$ , and  $h_a$ , the dimensional boiling time can be calculated by multiplying the corresponding value of  $\tau$  in panel (a) with the value of  $t_{\text{nuc}}/\tau$  obtained from panel (b).

experimental configuration involves creating a spherical inclusion in a hydrogel or elastic material, filling it with liquid, and then increasing the temperature past the boiling point. This is similar to the approach taken by Cline and Anthony [41] to study the vapourisation of water inclusions in salt crystals. Applying our theory to their data is difficult because nucleation occurs at such high temperatures that volumetric expansion due to changes in the temperature and composition of the material becomes relevant. Moreover, plastic deformations occur in the salt, which are outside the scope of the purely elastic mechanical responses considered here. Nevertheless, the experiments by Cline and Anthony demonstrate a feasible approach for probing the elasticity dependence of the boiling temperature.

## 5. Conclusions

Motivated by the problem of HTB massecuite, we develop a simple extension of classical nucleation theory that accounts for the elastic energy of superheated network fluids. Our results explicitly show that additional superheating is required to induce nucleation when the fluid has an elastic component. Furthermore, we find that the temperature at which nucleation occurs is linearly dependent on the shear modulus of the fluid. These results are consistent and analogous with those of Gent and Tompkins [10], who found the same relationship between the critical pressure for nucleation in supersaturated elastomers and their shear modulus. However, further experiments are required to validate the theory proposed here. Due to the generality of our problem formulation, we believe the results can be straightforwardly applied to

other experimental systems.

The results from our analysis show that the presence of elasticity can significantly impact the boiling characteristics of massecuite. Elasticity can directly suppress boiling by increasing the nucleation temperature to ranges that are not achievable in production-scale pans. Furthermore, elasticity can increase the size of nucleated vapour bubbles, making them more likely to become trapped in the polysaccharide network that permeates HTB massecuite. The increased viscosity of HTB massecuite may act in conjunction with elasticity to negatively influence the boiling dynamics by retarding the subsequent growth of nucleated vapour bubbles to millimetre scales. Given the lack of experimental data on the boiling temperature and viscoelastic response of HTB massecuite, it would be very insightful to run a set of experiments that aim to measure these quantities. Such a study would provide a means of validating the theory developed in this paper and provide refined estimates of the influence of elasticity on massecuite boiling. Based on our theoretical results of nucleation, we can conclude that future studies on HTB massecuite should focus on strategies for avoiding the formation of the polysaccharide network or methods for destroying it once it has formed.

By modelling the transport of heat from the calandria into massecuite, we find that variations in the thermal conductivity do not substantially alter the time required to reach the boiling (or nucleation) temperature. Reductions in the heat transfer coefficient can lead to significant increases in this boiling time, but this seems to only be problematic when the nucleation temperature is increased beyond the standard value of 70 °C. For example, the predicted boiling time for massecuite that boils at 70 °C ranges from 0.1 s to 10 s. This variation is likely insignificant. However, for massecuite that boils at 100 °C, the range of boiling times is from 10 s to 1000 s, which is significant. Given this large variation in boiling time, prior knowledge of the heat transfer coefficient, obtained, for example, from a pre-processing procedure, would help ensure the massecuite is heated for a sufficient period of time. Increases in boiling time could be compounded by potential fouling at the calandria wall, which would lead to further reductions in the heat transfer coefficient. Further investigations into the role of fouling and methods for combating it could also prove to be beneficial.

Finally, we note that in the modelling framework developed here, it has been assumed that the only volatile component in massecuite is water. However, as discussed in Eggleston *et al.* [4], there have been reports of microbes producing ethanol in HTB massecuite. The standard boiling temperature of ethanol is about 78 °C. However, in practice, the boiling temperature of ethanol would be even lower due to the pan boiler being held below atmospheric pressure. Thus, it is likely that any ethanol contained within HTB massecuite would boil first, and this may impact the subsequent boiling of water. After reviewing the literature, it appears that the physico-chemical impact of ethanol in massecuite has not received much attention, so this could be another fruitful area of future investigation.

### *Conflict of interest*

The authors declare that there is no conflict of interest.

### *Acknowledgements*

I. M. acknowledges the travel support from a Science Foundation Ireland grant SFI/13/IA/1923. M. H. has been partially funded by the CERCA Programme of the Generalitat de Catalunya and has received funding from the European Union's Horizon 2020 research and innovation programme under the Marie Skłodowska-Curie grant agreement No. 707658. The authors would like to thank Richard C. Loubser for bringing this problem to our attention and for reading an earlier version of this manuscript. Furthermore, we would like to extend our gratitude to Prof. David P. Mason for organising the Mathematics in Industry Study Group (MISG) at the African Institute for Mathematical Sciences, where work on this problem began.

## **Appendix A. Evaluation of the elastic energy**

As shown in (6), evaluating the elastic energy  $U_e$  requires calculating the integral

$$\mathcal{E} = \int_{\lambda_0^{-1}}^{\infty} \mathcal{W}(\tilde{I}_1, \tilde{I}_2) \tilde{R}^2 d\tilde{R}. \quad (\text{A.1})$$

For the incompressible Mooney–Rivlin materials considered here, the strain energy density  $\mathcal{W}$  can be written as

$$\mathcal{W}(\tilde{I}_1, \tilde{I}_2) = \frac{\mu(1-\mathcal{M})}{2} \left[ \left( \frac{\partial \tilde{r}}{\partial \tilde{R}} \right)^2 + 2 \left( \frac{\tilde{r}}{\tilde{R}} \right)^2 - 3 \right] + \frac{\mu\mathcal{M}}{2} \left[ \left( \frac{\tilde{r}}{\tilde{R}} \right)^4 + 2 \left( \frac{\tilde{r}}{\tilde{R}} \frac{\partial \tilde{r}}{\partial \tilde{R}} \right)^2 - 3 \right]. \quad (\text{A.2})$$

where  $\tilde{r}(R) = (\tilde{R}^3 + 1 - \lambda_0^{-3})^{1/3}$ . Using the parameters in Table 1, we find  $\lambda_0 \simeq 9.8$ . Due to the largeness of  $\lambda_0$ , asymptotic methods (see, for example, Ref. [42, Chap. 3.4]) can be used to evaluate the integral. We find that

$$\mathcal{E} \simeq \frac{\mu}{2} \left[ (1-\mathcal{M}) \left( \frac{5}{3} - \frac{2}{\lambda_0} \right) + \mathcal{M} \left( \lambda_0 - \frac{2}{3} \right) \right]. \quad (\text{A.3})$$

To verify the accuracy of (A.3), we compare it against numerical calculations of (A.1) using the `integral` function in Matlab, taking  $\mu = 10$  kPa. In Fig. A.8 (a), we plot  $\mathcal{E}$  as a function of the inverse stretch  $\lambda_0^{-1}$  for different values of the Mooney–Rivlin parameter  $\mathcal{M}$ . The lines correspond to the numerical calculation of (A.1) while circles denote the asymptotic approximation given by (A.3). For each of the considered values of  $\mathcal{M}$ , we see that the results from the numerical calculation and asymptotic approximation are virtually superimposed. This suggests that the analytical approximation (A.3) gives an extremely accurate prediction of the full integral when the radial stretch is large. From the figure, we see that  $\mathcal{E}$  is mostly unaffected by changes in  $\lambda_0^{-1}$  if  $\mathcal{M} = 0$ , corresponding to neo-Hookean materials. For Mooney–Rivlin materials ( $\mathcal{M} > 0$ ), we see that  $\mathcal{E}$  decreases with increasing  $\lambda_0^{-1}$ . This reflects the fact that the elastic energy decreases as the

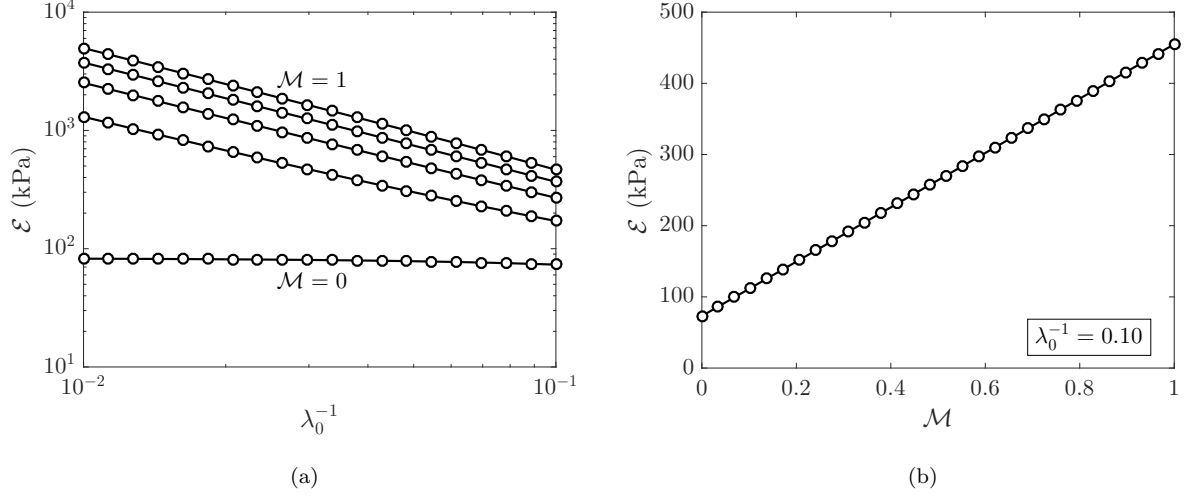


Figure A.8: (a) Variation in  $\mathcal{E}$  with inverse stretch  $\lambda_0^{-1}$  for  $\mathcal{M} = 0, 0.25, 0.50, 0.75$ , and  $1.0$ . (b) Dependence of  $\mathcal{E}$  on the Mooney–Rivlin parameter  $\mathcal{M}$  for a fixed value of  $\lambda_0^{-1} = 0.10$ . The lines in both panels have been obtained by numerically evaluating (A.1). Circles correspond to the asymptotic approximation (A.3). A value of  $\mu = 10$  kPa was used.

volumetric expansion of the gas and hence the deformation of the surrounding fluids is reduced. In Fig. A.8 (b), we plot  $\mathcal{E}$  as a function of  $\mathcal{M}$  for a fixed value of  $\lambda_0^{-1} = 0.10$  ( $\lambda_0 = 9.8$ ). The agreement between the asymptotic approximation and numerical calculations is again excellent. Both solutions show that  $\mathcal{E}$  and hence the elastic energy  $U_e$  linearly increase with the parameter  $\mathcal{M}$ .

## Appendix B. Reduction of the thermal model

Due to the large effective heat transfer coefficient,  $\alpha \gg 1$ , the initial heating of massecuite is confined to a thin region near the calandria wall. The localised and rapid nature of the heating process can be exploited to simplify the governing equations and determine how the boiling time  $t_{\text{nuc}}$  scales with the parameters of the system. We begin with the non-dimensional model given by (15) and introduce a rescaling of the variables that focuses on the transient heating that occurs in a thin region near the heated surface (at dimensionless position  $\hat{r} = 1$ ). This rescaling is given by  $\hat{t} = \alpha^{-2}\bar{t}$ ,  $\hat{r} = 1 - \alpha^{-1}\bar{r}$ , and  $\hat{u}(\hat{r}, \hat{t}) = \bar{u}(\bar{r}, \bar{t})$ . Using this rescaling in (15) and taking the limit as  $\alpha \rightarrow \infty$  results in the simplified model given by

$$\frac{\partial \bar{u}}{\partial \bar{t}} = \frac{\partial^2 \bar{u}}{\partial \bar{r}^2}, \quad (\text{B.1a})$$

with

$$\frac{\partial \bar{u}}{\partial \bar{r}} = -(1 - \bar{u}), \quad \bar{r} = 0, \quad (\text{B.1b})$$

$$\bar{u} \rightarrow 0, \quad \bar{r} \rightarrow \infty, \quad (\text{B.1c})$$

$$\bar{u} = 0, \quad \bar{t} = 0. \quad (\text{B.1d})$$

The rescaled boiling time is denoted by  $\tau$  and it satisfies the equation

$$\bar{u}(0, \tau) = \hat{u}_{\text{nuc}} = (T_{\text{nuc}} - T_a)/(T_s - T_a). \quad (\text{B.2})$$

Equation (B.2) shows that  $\tau$  will only depend on the nucleation temperature  $T_{\text{nuc}}$  as the thermal parameters have been scaled out of the model. By undoing the non-dimensionalisation, the dimensional boiling time,  $t_{\text{nuc}}$ , is given by

$$t_{\text{nuc}} = \tau(T_{\text{nuc}}) \frac{\rho_f c_p k}{h_a^2}. \quad (\text{B.3})$$

Strictly speaking, the reduced model (B.1) and the boiling time (B.3) are approximations that are valid when the effective heat transfer coefficient  $\alpha = kR_b/h_a$  is large. To confirm that the expression for the boiling time given by (B.3) is valid over the relevant range of  $\alpha$  between 13 and 115, we compare the values of  $\tau$  computed from (B.1)–(B.2) to equivalent values obtained by numerically solving the full dimensionless model (15)–(16). The equivalent value of  $\tau$  is obtained from (15)–(16) using the relationships  $\tau = \hat{t}_{\text{nuc}} \alpha^2 = t_{\text{nuc}} h_a^2 / (\rho_f c_p k)$ . Figure B.9 compares the variation in  $\tau = t_{\text{nuc}} h_a^2 / (\rho_f c_p k)$  with the nucleation temperature  $T_{\text{nuc}}$  predicted from the reduced model (B.1) and the full dimensionless model (15) using  $\alpha = 13$  and  $\alpha = 115$ . There is good agreement between the reduced and full models. In the case of  $\alpha = 115$ , the results are virtually indistinguishable.

## References

- [1] South African Sugar Association, Industry overview, [http://www.sasa.org.za/sugar\\_industry/IndustryOverview.aspx](http://www.sasa.org.za/sugar_industry/IndustryOverview.aspx), access Date: January 31, 2018.
- [2] American Sugar Cane League, Industry info, <http://www.amscl.org/industry-info>, access Date: January 31, 2018.
- [3] L. Echeverri, S. Acharya, P. Rein, Momentum interaction in buoyancy-driven gas–liquid vertical channel flows, *International Journal of Heat and Mass Transfer* 53 (9-10) (2010) 2284–2293.
- [4] G. Eggleston, G. Côté, C. Santee, New insights on the hard-to-boil massecuite phenomenon in raw sugar manufacture, *Food Chemistry* 126 (1) (2011) 21–30.
- [5] K. C. Koster, P. L. M. Vermeulen, M. A. Getaz, G. R. E. Lionnet, Some notes on abnormal processing difficulties during spring, in: *Proceedings of the South African Sugar Technologists Association*, Vol. 66, 1992, pp. 127–130.
- [6] M. Saska, Heat transfer rates in boiling of cane syrups and molasses and the phenomenon of hard-to-boil massecuites, in: *Proceedings of the Sugar Industry Technologists Meeting*, Australia, Vol. 62, 2003, pp. 175–187.
- [7] E. Duffaut, M. A. Godshall, Molecular probes for assessing boiling difficulties, in: *Proceedings of the Sugar Processing Research Conference*, 2004, pp. 403–416.

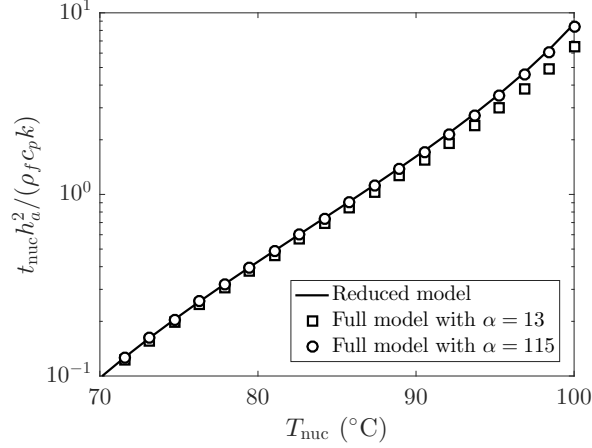


Figure B.9: Comparison of the rescaled boiling time  $\tau = t_{\text{nuc}} h_a^2 / (\rho_f c_p k)$  computed as a function of the nucleation temperature  $T_{\text{nuc}}$  using the reduced model (B.1)–(B.2) and the full dimensionless model (15)–(16) using  $\alpha = 13$  and  $\alpha = 115$ .

- [8] H. J. Maris, Introduction to the physics of nucleation, *Comptes Rendus Physique* 7 (9-10) (2006) 946–958.
- [9] R. F. Tournier, Predicting glass-to-glass and liquid-to-liquid phase transitions in supercooled water using classical nucleation theory, *Chemical Physics* 500 (2018) 45–53.
- [10] A. Gent, D. Tompkins, Nucleation and growth of gas bubbles in elastomers, *Journal of Applied Physics* 40 (6) (1969) 2520–2525.
- [11] C. Stewart, Nucleation and growth of bubbles in elastomers, *Journal of Polymer Science Part B: Polymer Physics* 8 (6) (1970) 937–955.
- [12] K. Y. Kim, S. L. Kang, H.-Y. Kwak, Bubble nucleation and growth in polymer solutions, *Polymer Engineering and Science* 44 (10) (2004) 1890–1899.
- [13] G. Guéna, J. Wang, J.-B. dEspinose, F. Lequeux, L. Talini, Boiling of an emulsion in a yield stress fluid, *Phys. Rev. E* 82 (5) (2010) 051502.
- [14] G. Hetsroni, M. Gurevich, A. Mosyak, R. Rozenblit, Z. Segal, Boiling enhancement with environmentally acceptable surfactants, *Int. J. Heat Fluid Flow* 25 (5) (2004) 841–848.
- [15] N. Y. Rapoport, A. L. Efros, D. A. Christensen, A. M. Kennedy, K.-H. Nam, Microbubble generation in phase-shift nanoemulsions used as anticancer drug carriers, *Bubble Sci. Eng. Tech.* 1 (1-2) (2009) 31–39.
- [16] K. Rykaczewski, A. Phadnis, Could use of soft surfaces augment onset of nucleate boiling?, *Nanoscale Microscale Thermophys. Eng.* (2018) 1–9.
- [17] A. D. Maxwell, C. A. Cain, T. L. Hall, J. B. Fowlkes, Z. Xu, Probability of cavitation for single ultrasound pulses applied to tissues and tissue-mimicking materials, *Ultrasound in medicine & biology* 39 (3) (2013) 449–465.
- [18] E. Vlaisavljevich, K.-W. Lin, A. Maxwell, M. T. Warnez, L. Mancia, R. Singh, A. J. Putnam, B. Fowlkes, E. Johnsen, C. Cain, et al., Effects of ultrasound frequency and tissue stiffness on the histotripsy intrinsic threshold for cavitation, *Ultrasound in medicine & biology* 41 (6) (2015) 1651–1667.
- [19] R. Oguri, K. Ando, Cavitation bubble nucleation induced by shock-bubble interaction in a gelatin gel, *Physics of Fluids* 30 (5) (2018) 051904.
- [20] F. Larché, J. W. Cahn, A linear theory of thermochemical equilibrium of solids under stress, *Acta Metallurgica* 21 (8) (1973) 1051–1063.
- [21] M. Blander, J. Katz, Bubble nucleation in liquids, *AIChE Journal* 21 (5) (1975) 833–848.

- [22] R. W. Hartel, R. Ergun, S. Vogel, Phase/state transitions of confectionery sweeteners: Thermodynamic and kinetic aspects, *Comprehensive Reviews in Food Science and Food Safety* 10 (1) (2011) 17–32.
- [23] L. F. Echeverri, Measurements and computations of the flow in full-scale sugar evaporative-crystallizers and in lab-scale models., Ph.D. thesis, Louisiana State University (May 2007).
- [24] P. D. Howell, G. Kozyreff, J. R. Ockendon, *Applied Solid Mechanics*, Cambridge University Press, 2009.
- [25] C. Shen, J. Simmons, Y. Wang, Effect of elastic interaction on nucleation: I. Calculation of the strain energy of nucleus formation in an elastically anisotropic crystal of arbitrary microstructure, *Acta Materialia* 54 (20) (2006) 5617–5630.
- [26] P. H. Leo, R. Sekerka, The effect of elastic fields on the morphological stability of a precipitate grown from solid solution, *Acta Metallurgica* 37 (12) (1989) 3139–3149.
- [27] J. Guyer, P. Voorhees, Morphological stability of alloy thin films, *Physical Review Letters* 74 (20) (1995) 4031.
- [28] T. J. Bruno, P. D. Svoronos, *CRC Handbook of Basic Tables for Chemical Analysis*, CRC Press, 2010.
- [29] G. W. C. Kaye, T. H. Laby, *Tables of physical and chemical constants: and some mathematical functions*, Longmans, Green and Company, 1921.
- [30] W. Wagner, A. Pruss, International equations for the saturation properties of ordinary water substance, *Journal of Physical and Chemical Reference Data* 22 (3) (1993) 783–787.
- [31] M. Asadi, *Beet-sugar handbook*, John Wiley & Sons, 2006.
- [32] C. B. P. Finn, *Thermal Physics: Second Edition*, CRC Press, 1993.
- [33] J. R. Cooper, R. B. Dooley, IAPWS Release on surface tension of ordinary water substance, International Association for the Properties of Water and Steam (IAPWS), Charlotte, NC 2.
- [34] R. Gaudron, M. Warnez, E. Johnsen, Bubble dynamics in a viscoelastic medium with nonlinear elasticity, *J. Fluid Mech.* 766 (2015) 54–75.
- [35] F. C. Larché, J. W. Cahn, Thermochemical equilibrium of multiphase solids under stress, *Acta Metallurgica* 26 (10) (1978) 1579–1589.
- [36] F. C. Larché, J. W. Cahn, The interactions of composition and stress in crystalline solids, *J. Res. Natl. Bur. Stand.* 89 (6) (1984) 467–500.
- [37] Y. Wang, T. Truong, B. Wang, S. Prakash, B. Bhandari, Effects of maltodextrin powder addition on the rheological and thermal properties of molasses, *Sugar Tech* 20 (5) (2018) 574–584.
- [38] J. H. Han, C. Dae Han, Bubble nucleation in polymeric liquids. II. Theoretical considerations, *J. Polym. Sci., Part B: Polym. Phys.* 28 (5) (1990) 743–761.
- [39] M. Doi, *Introduction to Polymer Physics*, Oxford University Press, 1996.
- [40] Y. H. Bae, T. Okano, S. W. Kim, Temperature dependence of swelling of crosslinked poly (N, N'-alkyl substituted acrylamides) in water, *J. Polym. Sci., Part B: Polym. Phys.* 28 (6) (1990) 923–936.
- [41] H. Cline, T. Anthony, Vaporization of liquid inclusion in solids, *Philos. Mag.* 24 (192) (1971) 1483–1494.
- [42] E. J. Hinch, *Perturbation Methods*, Cambridge University Press, 1991.